Frequency modulated continuous wave and time of flight LIDAR with single photons: a comparison

THEODOR STAFFAS,* [ID] ALI ELSHAARI, [ID] AND VAL ZWILLER

KTH Royal Institute of Technology, Department of Applied Physics, Albanova University Centre, Roslagstullbacken 21, 106 91 Stockholm, Sweden
*tstaffas@kth.se

Abstract: In this study, we compare the two prominent *Light Detection and Ranging* (LIDAR) technologies: *Frequency Modulated Continuous Wave* (FMCW) and *Time of Flight* (ToF). By constructing a setup capable of performing both LIDAR methods at the single photon level using a *Superconducting Nanowire Single Photon Detector* (SNSPD), we compare the accuracy and investigate the dependence of the resulting images and accuracy on the signal power and the corresponding signal to noise ratio. We demonstrate that both LIDAR methods are able to reconstruct 3D environments with a signal-to-noise ratio as low as 0.03. However, the accuracy of FMCW LIDAR is shown to degrade in the low photon regime, while ToF LIDAR accuracy is shown to be stable across the same range. Lastly, we use a median de-noising convolution filter to effectively combat the typical "salt and pepper" noise found in LIDAR images, further enhancing the performance of both methods.

1. Introduction

Light Detection and Ranging (LIDAR) is a remote optical sensing technique to measure the distance to an object. The technology was originally pioneered by militaries around the world and one of the first implementations of LIDAR was as range finders, produced by Ericsson AB, for Swedish coastal guns in 1968 [1], a mere eight years after the first laser was constructed. Since then, LIDAR has also found many civilian applications such as automation, robotics [2], medicine [3,4], forestry [5], archaeology [6], space mapping [7], and climate research [8,9] to name a few. The impact of the technology on our society is hard to overstate.

Originally, LIDAR systems relied on *Time of Flight* (ToF) measurements, where laser pulses are directed towards an object, reflected, and the travel time is measured to determine the distance [10]. This technique is effective and widely used. It can achieve mm resolution over km distances [9] and the implementation, as well as data analysis of a ToF LIDAR system is relatively simple compared to other LIDAR methods. It also has distinct drawbacks: it is susceptible to environmental background interference and imposes demanding requirements on the system components; the laser pulses, detectors, and timing electronics must all achieve picosecond operation to reach millimeter-level distance resolution [11,12]. An alternative approach to LIDAR is the *Frequency Modulated Continuous Wave* (FMCW) LIDAR [13], which measures the beat frequency between a probe signal and a local reference from a frequency-swept continuous laser to determine the distance to an object [14]. This approach offers several advantages compared to ToF LIDAR, including inherent insensitivity to interference from non-coherent sources, i.e., daylight [14,15], and the ability to simultaneously measure velocity and distance, rather than tracking changes in position over time [16]. The use of continuous wave instead of pulsed lasers also significantly decreases the demands on the laser and readout electronics, compared to those for ToF LIDAR, resulting in potential cost reductions for the system [11]. Continuous wave

lasers also allow for higher average output power while adhering to eye-safety standards, which increases the range of a system.

In both LIDAR methods, the fundamental information carriers are the photons used to probe the system, and to maximize the range or sensitivity of a system, we must operate at the single photon level. Previous work exists comparing the strengths and drawbacks of the two techniques using classical detectors [14] but not in the photon counting regime. In this project, we construct a setup capable of performing both FMCW and ToF LIDAR with a photon counting detecor and compare the two techniques' performance under identical environmental conditions and comparable measurement settings. We investigate and compare the accuracy as well as the ability of the two approaches to image 3D environments with progressively weaker reflected signals. Lastly, we attempt to improve the resulting images by applying median de-noising filters.

For this we utilize a *Superconducting Nanowire Single Photon Detector* (SNSPD). As the name suggests, this detector is composed of a nanowire made from superconducting material which is cooled below its critical temperature and biased near its critical current. When a photon is absorbed, it disrupts the superconducting state, and the nanowire transitions to the resistive state, causing a voltage pulse that is recorded as a single photon detection event [17,18]. The use of SNSPDs in ToF LIDAR is long-established [17,19] as they offer numerous advantages compared to other single photon detectors, such as *Avalanche Photo-Diodes* (APDs) [20,21]. These advantages include picosecond time jitter, high count rates, nanosecond dead time, low dark count rates, absence of after pulsing, and near-unity detection efficiency in the near-infrared [12,22–25]. The latter of these allows for the use of infrared lasers for LIDAR, which is beneficial due to the atmospheric transmission window. Implementing SNSPDs in ToF LIDAR also increases the range and resolution of the system while still using weak and therefore eye-safe laser powers, a detailed comparison of LIDAR using SNSPDs and APDs can be found in [21]. SNSPDs also allow for the use of longer, infrared wavelengths, because unlike photo-multiplier tubes or APDs, SNSPDs are not limited by any semiconductor band gap and have shown great detection efficiency up to and beyond 2 microns [10]. The use of SNSPDs in FMCW LIDAR, while tried [20], is not as established and the advantages are not equally investigated as for ToF: however, the superior performance of the SNSPDs still hold true. Unlike APDs, which may face challenges such as inferior timing resolution and susceptibility to dark counts noise at telecom wavelengths, SNSPDs operate without the need for gating. This is a significant advantage for FMCW LIDAR, where the continuous wave nature of the signal benefits from the free-running mode of SNSPDs. Moreover, the system efficiencies of SNSPDs, reaching up to 99%, contribute to improved overall sensitivity and accuracy in FMCW ranging applications [22,25].

2.   Theory and experimental setup

The experimental setup constructed for this project is shown in Fig. 1(a) and using this, we are able to perform both single photon FMCW and ToF LIDAR. For the sake of clarity and simplicity, we discuss the two methods separately and compare the results, but crucial in both is the SNSPD, which is cryogenically cooled to 2.6 K, has 80% detection efficiency at 1550 nm, with 19 ps timing jitter, dead time < 10 ns, a dark count rate < 100 Hz, and a maximum countrate of 5 MHz.

2.1.   FMCW LIDAR

To perform FMCW LIDAR with the system in Fig. 1(a) we use a continuous wave laser, coupled through a variable attenuator into a free-space setup where the beam is collimated and subsequently split by *beamsplitter 1* (BS1). The reflected beam serves as a local reference signal, Tx, transmitted to an SNSPD through an attenuator and BS3. The transmitted beam serves as a probe signal and is directed to a set of galvo mirrors by BS2. The galvo steers the laser beam across the environment by controlling the pitch and yaw with $\pm 20^o$ optical angle. The probe is reflected from a target and the reflected signal, Rx, travels back through BS2 and interferes
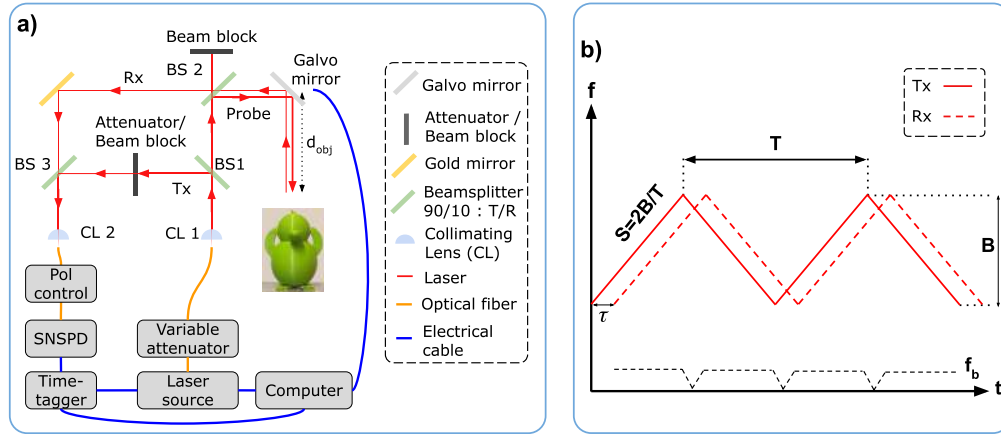
Fig. 1. a) Optical setup for both FMCW and ToF LIDAR. For FMCW LIDAR, a continuous laser is coupled to the free-space setup where it is split by BS2. The first signal, Tx, is coupled by BS1 and BS3 along the shortest path to the detector through 60 dB attenuation. The second signal serves as a probe signal and is directed via BS2 to a galvo that scans the probe across an object. The signal reflected from the object, Rx, is recombined with Tx at BS3. To perform ToF LIDAR the continuous laser is swapped for a pulsed laser diode and the Tx path is blocked. The laser pulses travel to the object and are reflected to the SNSPD, which generates an electrical detection pulse recorded by a timetagger. The arrival time is then compared to the time of emission to determine the ToF of the reflected photon. b) Overview of the principle of FMCW LIDAR. The time delay between a local reference and a reflected signal causes a difference in frequency when linearly modulated, resulting in a beating signal with frequency f_b.

with Tx at BS3. The resulting signal is coupled through a polarization controller to an SNSPD that measures the single photon countrate. The inclusion of the polarization controller is to compensate for the polarization sensitivity of the SNSPD.

The output frequency of the laser is swept linearly over time using a triangular pattern with slope S, over a given bandwidth B, as shown in Fig. 1(b). Given that Tx and Rx travel different distances between splitting at BS2 and recombination BS3, they acquire a time delay, $\tau = \frac{d_{tot}}{c}$. Where c is the speed of light and d_{tot} is the sum of the internal distance of the setup, d_{in}, along with the distance between the galvo and the object, d_{obj}. This time delay and the laser frequency modulation cause a difference in the frequency of the two signals at BS3. Therefore, the resulting signal will exhibit a beating frequency, f_b, that is directly dependent on the time delay and therefore the total distance according to Eq. (1) [26].

$$f_b = |S|\tau = \frac{|S|d_{tot}}{c} = \frac{|S|(d_{in} + 2d_{obj})}{c} = f_0 + \frac{|S|2d_{obj}}{c} \qquad (1)$$

where we define f_0 as a frequency offset caused by the constant internal difference in travel distance of Tx and Rx in the setup. This offset is easily measured by placing an object directly at the output of the system. It is also important to note that Eq. (1) only holds for stationary objects and that for moving targets, compensating terms for the Doppler shift must be introduced [16], but this is outside the scope of this work.

In single photon FMCW LIDAR the detector measures the time-dependent single photon flux and the beating frequency is determined via Fourier transform. Therefore, the distance resolution, d_{res}, is determined by the frequency resolution of the Fourier transform, f_{res}, which relates to the integration time, t_{int}, following the relationship: $f_{res} = \frac{1}{t_{int}}$ [14]. By referring to Eq. (1) we

derive an expression of d_{res}, Eq. (2), based on t_{int}, which in the context of FMCW LIDAR should equal half the period of the laser chirp, denoted as T in Fig. 1(b). Notably, the resolution of the system is primarily determined by the frequency bandwidth of the laser [14]. This assumes ideal components and conditions, which only exist in theoretical work. In practice, nonlinear phase noise present in the laser modulation results in a spreading of the beating frequency and will negatively impact the distance resolution. Much work has been done on minimizing and compensating for the effect of nonlinear phase noise [16,27] but this requires additional hardware and signal analysis and is outside the scope of this article. Furthermore, in the low power signal regime, the performance of FMCW LIDAR is reduced due to an insufficient number of reflected photons to accurately determine the beating frequency [15,28].

$$d_{res} = \frac{f_{res}c}{2S} = \frac{c}{2St_{int}} = \frac{c}{2S\frac{T}{2}} = \frac{c}{2B} \tag{2}$$

Our continuous wave laser has a central wavelength of 1550 nm and can modulate its output frequency triangularly with a bandwidth, $B = 17.5$ GHz, and repetition frequency, $f_r = 100$ Hz, leading to a theoretical distance resolution $d_{res} = 8$ mm, according to Eq. (2), i.e., the temporal resolution of the system can be expressed as $\frac{1}{B} = 57$ ps. The laser's output is kept below 500 μW average power, i.e., with BS1 and BS2 in Fig. 1(a) the probe signal directed at the target has maximal average power < 500 nW, and with the variable attenuator, we can attenuate the probe signal below 50 nW. Which is several orders of magnitude below the threshold for eye safety set by the Swedish government [29]. The strength of the Tx signal in Fig. 1 was optimized to be roughly 1 M photons/second and was kept at this constant level in all measurements by controlling the attenuation in the Tx path.

2.2. ToF LIDAR

As stated in the introduction, ToF LIDAR determines the distance by measuring the travel time of laser pulses to the object, and our system is also able to perform these measurements. Only two modifications are required: swapping the continuous laser for a pulsed laser diode and fully blocking the Tx signal path. The laser diode outputs 1550 nm pulses with 70 ps *Full-Width at Half-Max* (FWHM) and a variable repetition rate, for all measurements we operated with 10 MHz repetition rate. The laser pulses are coupled through the variable attenuator to the free-space setup via a fiber, the probe signal is steered across the environment by the galvo mirrors, and the reflected Rx signal is coupled to the SNSPD, as seen in Fig. 1(a). The detection events of the SNSPD are recorded by the timetagger, with 10 ps time jitter, along with sync signals from the laser diode, marking the emission of each laser pulse. The time difference between the timestamp of a photon reflected from the target and the corresponding sync signal yields the photon time of flight, τ_{tof}. This value is directly proportional to the total distance traveled by the photon internally in the setup (including the optical fibers between the laser, setup, and detector) and the distance between the galvo and the object, according to Eq. (3).

$$\tau_{tof} = \frac{d_{tot}}{c} = \frac{d_{in} + 2d_{obj}}{c} = \tau_0 + \frac{2d_{obj}}{c} \tag{3}$$

where we similarly define τ_0 as an internal offset of the system caused by the constant distance traveled by the photons within the setup. This offset is easily measured by placing an object directly at the output of the galvo and we perform this calibration measurement once. It must also be noted that for ToF LIDAR, BS1 and BS3 in Fig. 1(a) are not necessary and in a dedicated ToF LIDAR setup these would be removed, but this would destroy the alignment of the Tx and Rx paths for FMCW LIDAR measurements and is therefore avoided.

The resolution of a ToF LIDAR is mainly limited by the timing jitter of the system components, t_{com} (laser, detector, and timetagger), and the temporal resolution of the laser

pulses, i.e. the FWHM. The total timing jitter of the system, t_{tot} can be descibred as: $t_{tot} = \sqrt{t_{det}^2 + t_{laser}^2 + t_{timetagger}^2 + FWHM_{laser}^2}$. The total timing jitter of our setup is roughly 70 picoseconds which equates to a theoretical 10 mm distance resolution.

3. Analysis

For both FMCW and ToF LIDAR the SNSPD and timetagger record the arrival time of each photon. For FMCW LIDAR we analyze the single photon countrate and for ToF LIDAR we analyze the difference in arrival time between laser sync signals and detected photons. The analysis of these data sets are described separately below.

3.1. FMCW

Figure 2(a) displays a sample of the data obtained in a FMCW LIDAR measurement to a stationary point. The measurement integration time was 5 ms and the photon countrate recorded by the SNSPD and timetagger is plotted in a histogram with 10 ns binsize. The binsize was chosen to match the dead time of the detectors to ensure at most a single detected event is present in each time bin. The countrate histogram is then transformed using the *Fast Fourier Transform* (FFT) to produce a *Power Spectral Density* (PSD) vs frequency plot that is normalized, shown in Fig. 2(b). Two filters are then applied to the PSD data: a digital low-frequency cutoff at 7.5 kHz to remove frequencies arising from possible internal reflections in the setup, and an amplitude filter of 0.5 to filter out spectral noise. From the filtered PSD data shown in Fig. 2(c) we extract the frequency of the peak value, f_{peak}, and the center of mass frequency, f_{com}, defined by Eq. (4).

$$f_{com} = \frac{\sum f_i * PSD_i}{\sum f_i} \tag{4}$$

where f_i and PSD_i are the frequency and corresponding PSD of the filtered Fourier data. Each value can be interpreted as the beating frequency, and thus be used to determine the distance of the target according to Eq. (1).
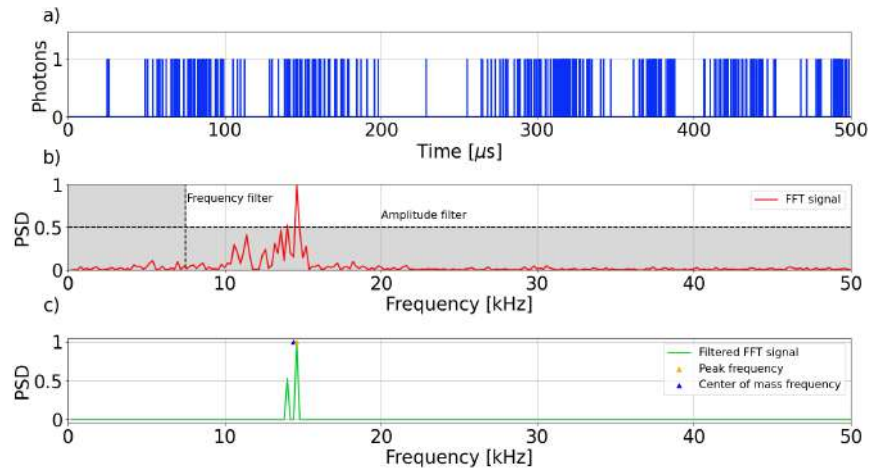

Fig. 2. a) A 500 μs sample of an FMCW LIDAR measurement to a fixed point with 5 ms integration time and 20 ps resolution timestamps. b) Fourier transform of the data in a), displaying the *Power Spectral Density* (PSD) vs frequency. c) A digital 7.5 kHz high-frequency cutoff filter as well as a 0.5 amplitude filter is applied to the data in b). From this filtered data, we extract two measurements of the beat frequency, the peak value, and the center of mass.

It must be mentioned that other frequency analysis algorithms relying on maximum-likelihood estimations have been proposed [30] and demonstrate improvements in the range estimations compared with using FFT analysis. Both algorithms, however, are shown to struggle in the photon starved signal regime [30]. Therefore, in this work, we have chosen to use the FFT approach based on its easier implementation.

3.2. ToF

Figure 3 displays the data collected in a ToF LIDAR measurement to a single point. The integration time was 5 ms and the travel time of the detected photons are recorded in a histogram with binsize 20 ps. The binsize was chosen to match the timing jitter of the detector. There are two distinct peaks: the first is due to a reflection in the setup and constantly present in all measurements and is therefore filtered out. The second peak is from the target and the location of the peak, τ_{peak}, can be used as the ToF to determine the distance according to Eq. (3). To further improve the measurement, we also fit a Gaussian curve to the second peak and use the center of the fitted curve, τ_{gauss}, as the ToF.
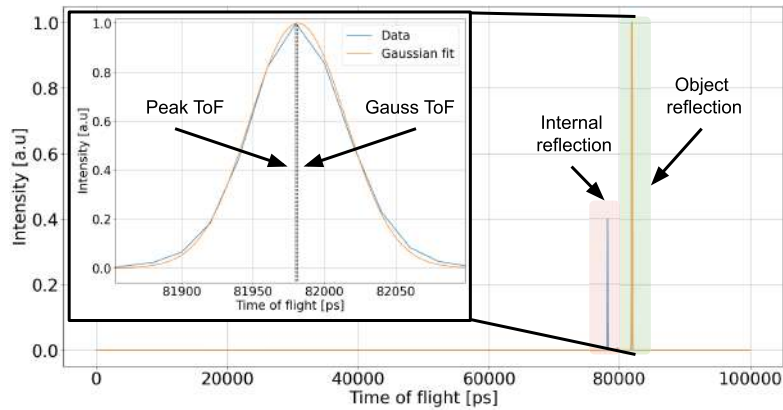
Fig. 3. Sample ToF LIDAR measurement to a fixed object. The data is displayed in a ToF histogram with two peaks: an internal reflection and the target reflection. The data is analyzed using two techniques: peak identification and Gaussian curve fitting, yielding two values of ToF.
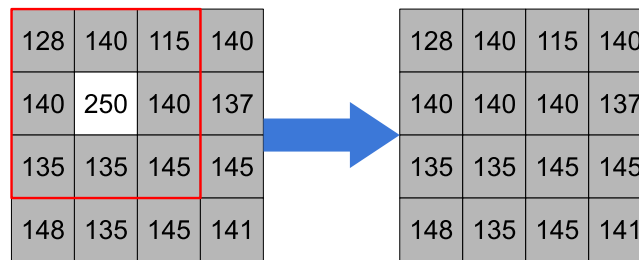
Fig. 4. Demonstration of a median convolution de-noising filter. In the example, one pixel is strongly deviating from its neighbors, indicating it might be a faulty measurement or damaged pixel. In an attempt to reduce the noise, each pixel is set as the median of its neighbors (We ignore the complications of the edge cases in this example).

3.3. Median de-noising filter

The median de-noising filter is a convolution filter designed to remove so-called "salt and pepper" noise from images. The principle is displayed in Fig. 4 where the 4x4-pixel image is relatively homogeneous except for one strongly deviating value. This type of noise is for example common in cameras with damaged pixels. To remove the noise a median convolution filter is applied, setting each pixel to the median value of its surrounding neighbors [31].

4. Results

4.1. Accuracy

To compare the accuracy of the LIDAR methods, we performed 4000 measurements to a single, stationary point 350 mm from the galvo, using both FMCW and ToF with 5 ms integration time for both methods. For the FMCW measurements, we extract both f_{com} and f_{peak} and for the ToF measurements, we extract τ_{peak} and τ_{gauss}. The results displayed in the boxplot in Fig. 5(a) demonstrate the difference in accuracy between the two methods as ToF LIDAR achieves higher accuracy compared to FMCW LIDAR. The average probe power then varied as to 500, 250, 100, and 50 nW, respectively, to investigate the accuracy dependency of the probe power, Fig. 5(b). The ToF accuracy is shown to be stable across all probe signals, at ±0.8 mm using Gaussian analysis, whereas the FMCW accuracy deteriorates at weaker probe signals to ±25 mm with 50 nW probe signal.
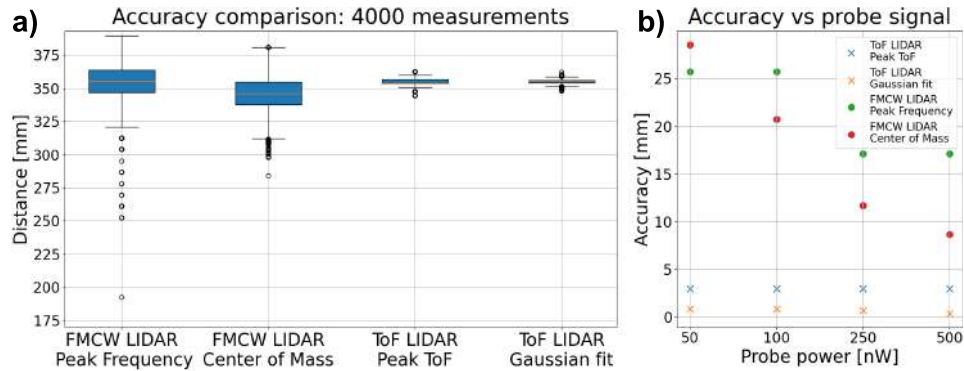
Fig. 5. a) Box plot of 4000 measurements performed to a stationary point using both FMCW and ToF LIDAR with 5 ms integration time to compare the resolution of the two methods. b) Accuracy of LIDAR methods vs average probe signal power.

4.2. 3D reconstruction and noise tolerance

To compare the ability of the two LIDAR methods to reconstruct 3D objects we scan the figurine in Fig. 6(a) using both FMCW and ToF. The figurine is scanned in a point-to-point (100 x 100) raster pattern with a 5 ms integration time per point. The SNSPD and timetagger continuously record the incoming signal, and to separate the measurements of the individual points, marker signals from the computer are injected into the data stream sent to the timetagger. For each point scanned we determine the distance based on the FMCW or ToF measurement. We also combine the distance with the angle of the galvo mirrors to calculate Cartesian x, y, z coordinates, resulting in Figs. 6(b) and 6(d). We observe that the FMCW image contains more noise than the ToF image and to reduce this we apply a median de-noising filter, producing Figs. 6(c) and 6(e). These results demonstrate that the filtering is effective at reducing the noise present in the LIDAR images.

Scanned object   FMCW LIDAR   De-noised image
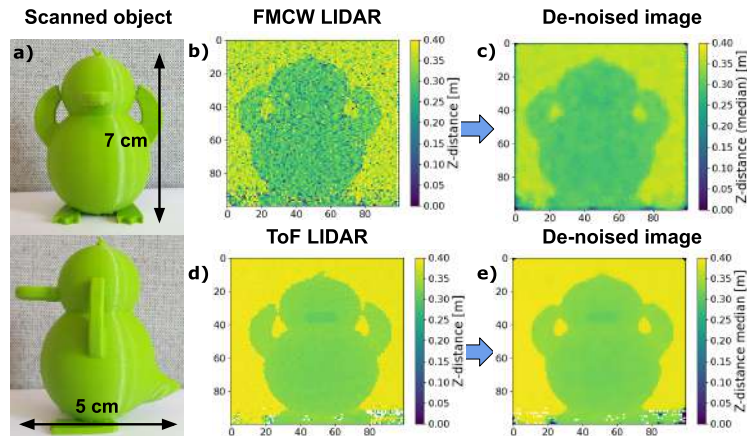
Fig. 6. Demonstration and comparison of a 3D reconstruction using FMCW and ToF LIDAR with identical parameters. a) 3D printed figurine of the Pokémon Psyduck (famous for its migraine-induced psychic powers). b) FMCW LIDAR measurement of the figurine. c) Median convolution filter, applied to the FMCW image. d) ToF LIDAR measurement of the figurine. e) Median convolution filter, applied to the ToF image.

To investigate the resilience of the LIDAR methods, we introduce a bright, broadband source of non-coherent noise next to the figurine (a candle) and scan it with decreasingly lower probe power and *Signal to Noise Ratio* (SNR). The average probe power is again set to 500, 250, 100, and 50 nW, respectively, yielding an SNR of 0.3, 0.15, 0.06, and 0.03. The noise source produced an average 500k photons/second background signal while a 500 nW probe yielded an average 150k photons/second reflected signal. The resulting de-noised images are shown in Fig. 7. Important to note: in the ToF measurement, due to the repetition frequency and the laser pulses FWHM, the peak power is ∼ 1000 times larger than the average probe signal but still within eye-safety limits.
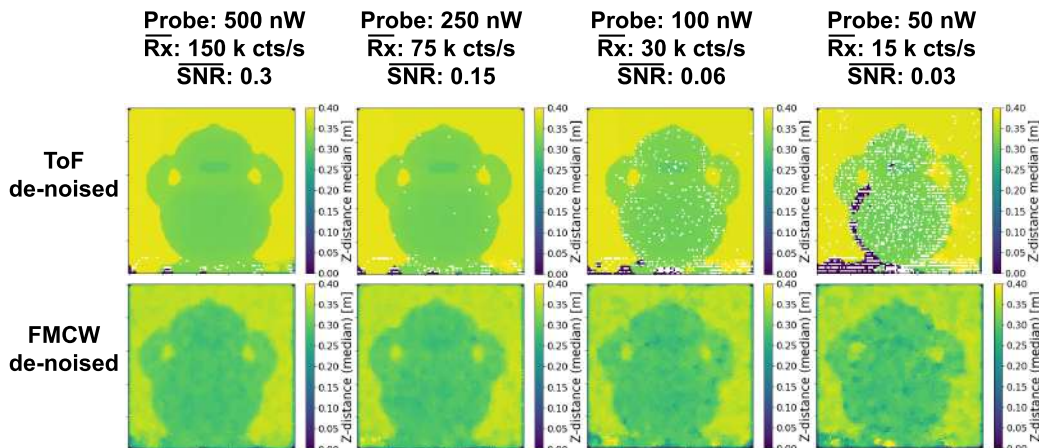
Fig. 7. Multiple LIDAR scans with progressively lower SNR. The SNR and Rx signal values are the average over the image. The top row displays the ToF measurements, and the bottom row the FMCW measurements. All images have been de-noised using an identical median convolution filter.

5. Conclusion

In this paper, we construct a system capable of performing FMCW and ToF LIDAR at the single photon level using an SNSPD and compare the performance of the two methods under identical environmental conditions. First, we compare the accuracy achieved by the two LIDAR methods and the results in Fig. 5(b) demonstrate that ToF achieves a better accuracy (±0.8 mm using Gaussian curve fitting) compared to FMCW LIDAR (±9 → ±25 mm). More importantly, the ToF accuracy is shown to be stable even for weaker probe signals where the FMCW LIDAR accuracy deteriorates. These results differ from the theoretical expectations that predicted ToF to achieve 10 mm accuracy and FMCW 8 mm. The reason for the ToF discrepancy is that while ToF LIDAR accuracy for a single detected photon is limited by the total timing jitter, it is not the ultimate limit when using multiple detection events. The ToF of reflected photons from a target are distributed in a Gaussian curve where the FWHM is determined by the total timing jitter and the central value is the true ToF. The accuracy of a ToF LIDAR is the precision with which the central value can be determined. This is why the accuracy is better than expected and why fitting a Gaussian curve to the data in Fig. 3 improves the accuracy as demonstrated by the results in Fig. 5(b). The discrepancy in FMCW accuracy with weaker probe signals is caused by insufficiently reflected photons to perform accurate FFT analysis. For stronger probe signals (500 nW) the accuracy is shown to be ±9mm, closer to the theoretical value. In this regime, the limiting factor is nonlinear phase noise in the modulated laser. The main conclusion of the results displayed in Fig. 5 is: for photon starved reflected signals, the ToF accuracy remains stable with weaker signals whereas the FMCW accuracy degrades. The numerical results are, of course, highly dependent on equipment specifications such as laser pulse width, detector timing jitter, frequency sweep rate, etc. Changes to these parameters can move the data points in Fig. 5(b) vertically, and an FMCW LIDAR system can be made that surpasses a ToF system, for example, by increasing the bandwidth of the laser frequency modulation, but the trend of degrading FMCW performance for low photon return signals will remain.

Second, we compare the impact weaker probe signals and lower SNR have on the ability of the LIDAR techniques to reconstruct 3D environments. The results in Fig. 7 demonstrate that both LIDAR methods are highly resilient to background noise given the same average probe power, identical integration time, and environmental conditions. The FMCW images produced contain more noise than those produced using ToF due to the difference in accuracy, especially with weaker probe signals. Using a median convolution filter does mitigate the effects of this, as shown in Fig. 6(b) and 6(c).

Disclosures. The author Val Zwiller is a co-founder of the company Single Quantum that provided the detection system used in this project. Others declare no conflicts of interest.

Data availability. All data underlying the results presented in this paper are available upon request.

Supplemental document. See Supplement 1 for supporting content.

References

1. V. Molebny, G. Kamerman, and O. Steinvall, "Laser radar: from early history to new trends," Electro-Optical Remote. Sensing, Photonic Technol. Appl. IV **7835**, 783502 (2010).
2. N. Mehendale and S. Neoge, "Review on lidar technology," SSRN ssrn.3604309, (2020).
3. M. G. Tanner, T. R. Choudhary, T. H. Craven, *et al.*, "Ballistic and snake photon imaging for locating optical endomicroscopy fibres," Biomed. Opt. Express **8**(9), 4077 (2017).
4. Z. Zhang, Y. Liu, T. Stephens, *et al.*, "Photonic radar for contactless vital sign detection," Nat. Photonics **17**(9), 791–797 (2023).
5. R. O. Dubayah and J. B. Drake, "Lidar Remote Sensing for Forestry," J. Forestry **98**(6), 44–46 (2000).
6. M. Balsi, S. Esposito, P. Fallavollita, *et al.*, "Preliminary archeological site survey by uav-borne lidar: A case study," Remote Sens. **13**(3), 332 (2021).
7. M. Wilkinson, U. Schreiber, I. Procházka, *et al.*, "The next generation of satellite laser ranging systems," J. Geodesy **93**(11), 2227–2247 (2019).

8. J. Larsson, J. Bood, C. T. Xu, *et al.*, "Atmospheric Co$_2$ sensing using scheimpflug-lidar based on a 157-μm fiber source," Opt. Express **27**(12), 17348 (2019).
9. A. McCarthy, X. Ren, A. D. Frera, *et al.*, "Kilometer-range depth imaging at 1550 nm wavelength using an ingaas/inp single-photon avalanche diode detector," Opt. Express **21**(19), 22098 (2013).
10. G. G. Taylor, D. Morozov, N. R. Gemmell, *et al.*, "Photon counting lidar at 23μm wavelength with superconducting nanowires," Opt. Express **27**(26), 38147 (2019).
11. M. Okano and C. Chong, "Swept source lidar: simultaneous fmcw ranging and nonmechanical beam steering with a wideband swept source," Opt. Express **28**(16), 23898 (2020).
12. B. Korzh, Q. Y. Zhao, J. P. Allmaras, *et al.*, "Demonstration of sub-3 ps temporal resolution with a superconducting nanowire single-photon detector," Nat. Photonics **14**(4), 250–255 (2020).
13. T. E. Honeycutt and W. F. Otto, "Fm-cw radar range measurement with a coz laser," IEEE J. Quantum Electron. **8**(2), 91–92 (1972).
14. B. Behroozpour, P. A. Sandborn, M. C. Wu, *et al.*, "Lidar system architectures and circuits," IEEE Commun. Mag. **55**(10), 135–142 (2017).
15. X. Huang, Y. Hong, Z.-P. Li, *et al.*, "Frequency-modulated continuous-wave 3d imaging with high photon efficiency," Opt. Lett. **47**(14), 3568–3571 (2022).
16. F. Zhang, L. Yi, and X. Qu, "Simultaneous measurements of velocity and distance via a dual-path fmcw lidar system," Opt. Commun. **474**, 126066 (2020).
17. C. M. Natarajan, M. G. Tanner, and R. H. Hadfield, "Superconducting nanowire single-photon detectors: Physics and applications," Supercond. Sci. Technol. **25**(6), 063001 (2012).
18. A. M. Pawlikowska, A. Halimi, R. A. Lamb, *et al.*, "Single-photon three-dimensional imaging at up to 10 kilometers range," Opt. Express **25**(10), 11919 (2017).
19. I. Esmaeil Zadeh, J. Chang, J. W. N. Los, *et al.*, "Superconducting nanowire single-photon detectors: A perspective on evolution, state-of-the-art, future developments, and applications," Appl. Phys. Lett. **118**(19), 190502 (2021).
20. J. Zhang, M. A. Itzler, H. Zbinden, *et al.*, "Advances in ingaas/inp single-photon detector systems for quantum communication," Light: Sci. Appl. **4**(5), e286 (2015).
21. R. H. Hadfield, J. Leach, F. Fleming, *et al.*, "Single-photon detection for long-range imaging and sensing," Optica **10**(9), 1124–1141 (2023).
22. D. V. Reddy, R. R. Nerem, S. W. Nam, *et al.*, "Superconducting nanowire single-photon detectors with 98% system detection efficiency at 1550 nm," Optica **7**(12), 1649 (2020).
23. D. Salvoni, M. Ejrnaes, L. Parlato, *et al.*, "Lidar techniques for a snspd-based measurement," J. Phys.: Conf. Ser. **1182**, 012014 (2019).
24. R. Jaha, F. Beutel, M. A. Wolff, *et al.*, "Decreasing snspd jitter to sub-3 ps upon increased photon illumination," in *CLEO* (Optica Publishing Group, 2023), paper SM4G.3.
25. J. Chang, J. W. N. Los, J. O. Tenorio-Pearl, *et al.*, "Detecting telecom single photons with 99.5 % system detection efficiency and high time resolution," APL Photonics **6**(3), 036114 (2021).
26. Y. Dong, Z. Zhu, X. Tian, *et al.*, "Frequency-modulated continuous-wave lidar and 3d imaging by using linear frequency modulation based on injection locking," J. Lightwave Technol. **39**(8), 2275–2280 (2021).
27. Z. Ding, C. Wang, K. Liu, *et al.*, "Distributed optical fiber sensors based on optical frequency domain reflectometry: A review," Sensors **18**(4), 1072 (2018).
28. Z. W. Barber, J. R. Dahl, T. L. Sharpe, *et al.*, "Shot noise statistics and information theory of sensitivity limits in frequency-modulated continuous-wave ladar," J. Opt. Soc. Am. A **30**(7), 1335–1341 (2013).
29. Arbetsmiljoverket, "Artificiell optisk strålning (afs 2009:7), föreskrifter - arbetsmiljöverket," (2019).
30. B. I. Erkmen, Z. W. Barber, and J. Dahl, "Maximum-likelihood estimation for frequency-modulated continuous-wave laser ranging using photon-counting detectors," Appl. Opt. **52**(10), 2008–2018 (2013).
31. A. C. Bovik, *The Essential Guide to Image Processing* (Academic Press, 2009).